INSTITUTE OF PHYSICS PUBLISHING JOURNAL OF MICROMECHANICS AND MICROENGINEERING

J. Micromech. Microeng. **16** (2006) 2121–2127 doi:10.1088/0960-1317/16/10/028

A low-energy, turning microvalve with high-pressure seals: scaling of friction

Lennart Bitsch[1,2], Jörg P Kutter[1], Torben Storgaard-Larsen[2] and Henrik Bruus[1]

[1] MIC—Department of Micro and Nanotechnology, Technical University of Denmark, DTU Bldg. 345 East, DK-2800 Kgs. Lyngby, Denmark
[2] Novo Nordisk A/S, Brennum Park, Hillerod, DK-3400, Denmark

E-mail: lbi@mic.dtu.dk

Received 24 April 2006, in final form 28 July 2006
Published 1 September 2006
Online at stacks.iop.org/JMM/16/2121

Abstract
We present the design, fabrication, testing and scaling characteristics of a silicone-based turning microvalve. Opening and closing are managed by turning a steel rod, with a diameter of 250 μm. The actuation energy for opening and closing the valve is 0.15 mJ, and when closed the valve withstands pressures higher than 0.7 MPa. The valve design in combination with studies of the scaling behavior of friction and sealing shows the feasibility of low-energy turning microvalves with a high-pressure seal. For an appropriate parameter range we show that the friction force scales linearly with the apparent contact area and with the relative radial displacement of the elastic channel walls. Finally, our results illustrate the necessity of parameter control in order to develop a robust valve with the benefits of down-scaling.

1. Introduction

For a number of years it has been predicted that microfluidic systems would significantly contribute to commercial success in various fields. One such field is drug delivery for which micropumps have been under development ever since the late 1970s [1] and up until today [2]. In a survey on the commercial opportunities of microfluidics, it was stated that one of the reasons for lacking or postponed success for applications in drug delivery was the immaturity of the technology [3]. One possible methodological approach to reach the required maturity level is *robust design*, which ensures optimal performance for a given range of parameters [4]. This well-established method, rarely used in microfluidics, does require predictability of the scaling behavior and parameter dependency. In the work presented here, we have chosen to focus on improving the performance of a microvalve by *model-based down-scaling*.

Furthermore, it has also been argued that the long development time of many microsystems is due to the mechanical properties of silicon, which for a long time has been the preferred material for microprocessing. However, as stated by Quake and Scherer [5], silicon is not the material most suitable for liquid handling, and the use of soft materials is going to have a tremendous impact on the commercialization of microfluidics. Therefore, the valve design reported herein relies on *soft, polymer-based materials*, in particular silicone rubber.

Valves are essential components for proper flow control in microfluidic systems. Two properties are especially vital for a valve in a portable microsystem: a low energy consumption and a near perfect sealing in the closed state with a high threshold pressure before breakthrough occurs. Attempting to fulfill both these requirements at the same time constitutes the central design challenge for making such microvalves. It is readily appreciated for drug delivery systems that the sealing properties of the valves involved are crucial, as even a small leakage may have fatal consequences. Consequently, a reliable *active valve* to precisely control delivery is desirable.

For a valve design utilizing a microplug polymerized inside the channel, Hasselbrink *et al* [6] have shown that static friction scales with the surface area and the normal force. The valves showed impressive sealing properties, but the in-channel polymerization proved cumbersome and, furthermore, a better understanding of sliding friction in microstructures was required. The application of this technology in an active valve was shown in [7]. In the development of a so-called gate-type valve, Frank *et al* [8] focused on low leakage and low

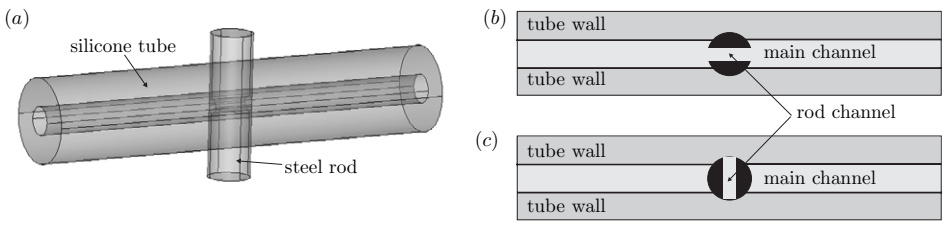

Figure 1. (*a*) Sketch of the turning microvalve with silicone walls and a steel rod. (*b*) The open state: the rod channel is parallel to the main channel. (*c*) The closed state: the rod channel is perpendicular to the main channel.

energy consumption. This particular type of valve shows good self-sealing properties, which means that an increased fluidic pressure increases the contact pressure and thus minimizes leakage. However, the rigid silicon used is not ideal for sealing purposes.

Here, we study a simple silicone-based turning (rotating) valve as sketched in figure 1. It is chosen primarily for its simplicity, its low energy consumption and its good sealing properties in the closed state. Energy is only consumed when the valve is switched between the open and the closed state. Moreover, energy consumption is further reduced by down-scaling the valve, since, as shown in this work, friction scales with surface area. The valve has good sealing properties in terms of a high threshold pressure for breakthrough, due to the elasticity of the silicone rubber channel walls and because in the closed state the passageway through the steel rod is positioned perpendicular to the main channel.

The paper is organized as follows. In section 2 we present two test systems, the plug setup, which is used to study the sealing properties of steel plugs in silicone microchannels and the related threshold pressures for leakage, and the torque setup, which allows us to study friction of rotating steel rods in contact with pierced silicone membranes. In particular, we examine how the friction force behaves when scaling down. In section 3, we present the design, fabrication and experimental test results of the turning microvalve. Finally, a conclusion is presented in section 4.

2. Two test setups for studying the sealing and scaling properties of friction

In this section, two experimental test setups for studying the basic sealing and friction properties of silicone-based microchannels are presented: the plug setup and the torque setup, respectively. These test setups have a high degree of similarity with the final turning valve, but due to their simpler geometry they allow for more clear-cut studies.

2.1. Theory and model for the plug setup

The sealing properties of silicone microchannels were studied using the plug setup sketched in figure 2. A wide steel plug of radius R_1 is inserted in a more narrow liquid-filled silicone tube of initial inner radius r_1. As $R_1 > r_1$, the inner wall of the elastic tube near the plug is displaced by the distance u_1, so that the tube now exerts a uniform pressure on the rod. This seals the channel for liquid flow for moderate over-pressures Δp at the inlet. As the inlet over-pressure is gradually increased the inner wall of the tube expands, initially only in the part

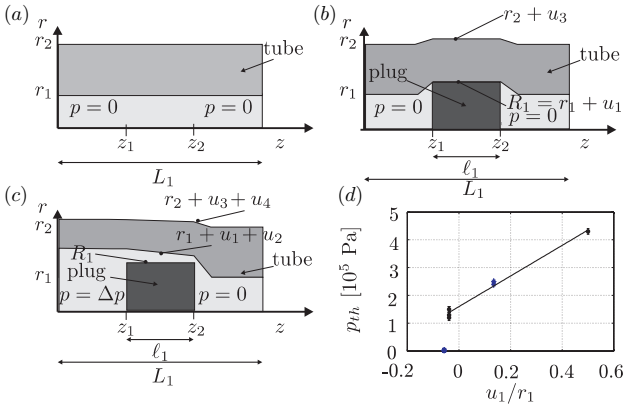

Figure 2. (*a*) Sketch of an axisymmetric elastic silicone tube (dark gray) of length L_1, inner radius r_1 and outer radius r_2. The tube is filled with water (light gray) at zero over-pressure $p = 0$. (*b*) The same tube after insertion of a wide steel plug of length ℓ_1 and radius $R_1 > r_1$. The plug causes displacements u_1 and u_3 of the inner and outer tube walls, respectively. (*c*) The inlet is pressurized to the over-pressure $p = \Delta p$ causing additional displacements u_2 and u_4 of the inner and outer tube walls, respectively. Note that Δp exceeds the threshold pressure and the seal is leaking. (*d*) The measured threshold pressure p_{th} versus u_1/r_1. Data are fitted with a linear regression line.

of the tube upstream from the plug. But, eventually, a certain threshold pressure p_{th} is reached where the tube also expands around the plug, by the additional displacement $u_2 > 0$. When this happens the seal is broken and a leakage flow bypassing the plug arises, see figure 2(*c*).

To obtain a simple expression for p_{th} as a function of the relative deformation u_1/r_1, we consider a cylindrical tube, subject to a uniform internal pressure p and zero external pressure. Assuming further that there is no displacement in the axial direction we get

$$p_{\text{th}} = k_c k_e \frac{u_1}{r_1} + p_0, \tag{1}$$

where k_c is an experimental correction factor, k_e is an elastic modulus and p_0 is the residual normal pressure for zero deformation arising from adhesion forces and boundary uncertainties. For the special case of tubes with a large relative width $(r_2 - r_1)/r_1$, it can be shown that $k_e = (2/3)\,E$, where E is Young's modulus. The discrepancy between this approximation and the numerical calculations is less than 1% for tubes used in these experiments. See [12] for a more detailed discussion of this approximation.

Table 1. Measured parameters for the four used plug setup geometries. For each of the two different tubes, characterized by the outer and inner diameters $2r_2$ and $2r_1$, respectively, two different plugs of diameter $2R_1$ have been employed.

Tube	$2r_2$ (μm)	$2r_1$ (μm)	$2R_1$ (μm)	$2R_1$ (μm)
Small bore	1200	260 ± 10	250 ± 10	390 ± 10
Large bore	3700	520 ± 10	490 ± 10	590 ± 10

2.2. Experimental realization of the plug setup

To conduct experiments on the sealing properties and the threshold pressure, we use a standard microfluidic measurement setup. A syringe pump feeds liquid into the system at a constant flow rate, while a pressure sensor measures the dynamic pressure at the inlet of the flow component, e.g., the plug setup. The outlet is always at atmospheric pressure. The inlet flow rates are given by the pump and the outlet flow rates are measured by collecting the effluent liquid in a waste beaker placed on a balance. For steady-state measurements without unaccounted for losses, these two flow rates should be equal. A PC sets the flow rate on the syringe pump and collects data from the electronic balance and the inlet pressure sensor through an RS232 interface and a DAQ-card, respectively.

2.3. Experimental results for the plug setup: sealing and threshold pressure

We have conducted 11 experiments with different plug and bore sizes. All used combinations of tubes and plugs are listed in table 1. In figure 2(*d*), a plot of the 11 measured threshold pressures p_{th} as a function of the relative displacement u_1/r_1 for the different plug setup geometries is shown. An abrupt increase from zero to above 0.16 MPa in p_{th} is seen as u_1/r_1 increases above -0.04. For the most negative value of u_1/r_1, i.e., the plug is smaller than the lumen of the tube, the threshold pressure is clearly seen to be zero, while for the points around $u_1/r_1 = -0.04$ a non-zero threshold pressure is found. This indicates that there may be some uncertainty in determining when $u_1/r_1 = 0$. A linear fit through the data points for the three largest deformations yields $k_c = 0.34$ and $p_0 = 0.16$ MPa, which is a relatively high value.

We conclude that p_{th} is independent of the contact area of the pressure seal, but, after an initial sudden jump to above 0.16 MPa as u_1/r_1 becomes positive, scales linearly with the relative displacement u_1/r_1.

2.4. Theory and model for the torque setup

In the rest of this section, using the so-called torque setup, we empirically study the scaling of friction between silicone rubber and steel. In contrast to friction between two hard substrates, rubber friction is mainly due to a bulk process and is therefore related to the viscoelastic properties of the rubber [9, 10]. During sliding, two processes can induce deformation and thereby internal friction in the rubber. These are adhesional forces and surface roughness, and for rough surfaces the adhesional contribution is reduced. Friction can be highly dependent on temperature. However, for the low sliding velocities employed in our work (less than 100 μm s^{-1}), temperature effects appear negligible [9].

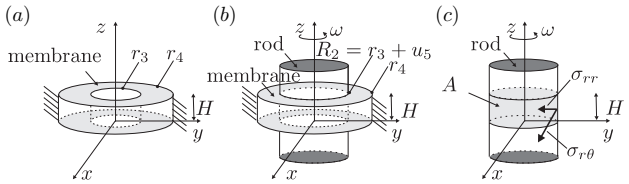

Figure 3. Sketch of the torque setup to study friction of a rotating steel rod piercing through an elastic silicone membrane. (*a*) A ring-shaped membrane of thickness H and inner and outer radii r_3 and r_4, respectively. The membrane is fixed at the outer radius. (*b*) After insertion of a rod of radius $R_2 > r_3$ the inner ring wall is displaced by u_5 and the rod rotates with angular velocity ω. (*c*) The friction stress $\sigma_{r\theta}$ and contact pressure σ_{rr} acting on the rod at the cylindrical contact area (light gray) between the membrane and the rod.

When referring to the interface between sliding objects, one typically distinguishes between the nominal area and the area of real contact. The nominal area is the apparent area which is observed without magnification, and the area of real contact is the actual contact area between the microscopic surface asperities. Due to a linearity between normal force and area of real contact, rubber friction is linearly dependent on the applied load. However, this is not true for very small loads, as friction does not decrease to zero at zero limit due to adhesional forces. At very large loads there is an upper limit for the linearity between area of real contact and load [9, 11].

To analyze the scaling properties of friction between silicone and a steel rod, we employ the torque setup depicted in figure 3. A ring-shaped elastic silicone membrane of thickness H and inner and outer radii r_3 and r_4, respectively, is fixed at the outer radius, see panel (*a*). A steel rod of radius $R_2 > r_3$ is inserted in the membrane hole thus displacing the inner ring wall by u_5, see panel (*b*). When the rod rotates relative to the silicone membrane with an angular velocity ω, it experiences a torque τ due to the friction forces acting on the cylindrical contact area between the rod and the membrane. The contact pressure σ_{rr} and the friction stress $\sigma_{r\theta}$ acting on the contact area, see panel (*c*), are modeled by standard expressions as

$$\sigma_{r\theta} = \eta \sigma_{rr}, \tag{2}$$

$$\sigma_{rr} = k_c k_e \frac{u_5}{r_3} + p_0, \tag{3}$$

where η is the friction coefficient, k_e is an elastic modulus equal to $(2/3)E$ and k_c is an experimentally determined correction factor, analogous to the one appearing in equation (1).

2.5. Experimental realization of the torque setup

The experimental realization of the torque setup is shown in figure 4. The core of the setup, as shown in panel (*b*), consists of a horizontal steel rod piercing two vertically arranged silicone membranes. The rod can be made to turn by rotating the two silicone membranes, which are connected to a stepper motor via a PMMA housing. A thin lever is mounted on the rod perpendicular to the rod's axis, such that when the rod is rotated the lever presses down onto an aluminum block placed on an electronic balance, see panel (*a*). In steady state the

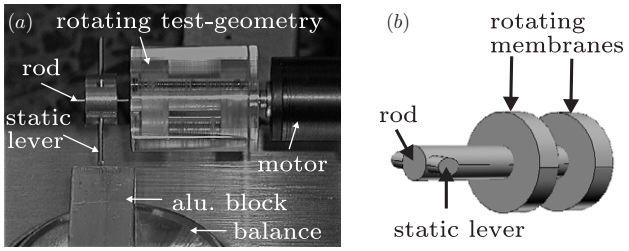

Figure 4. The balance-based torque setup and details on test geometry. (*a*) The torque test geometry is fixed on the motor axle and rotates with a set speed. A rod is hanging in two membranes inside the geometry, and on the rod is mounted a lever that rests on an aluminum block. The aluminum block is positioned on a balance. When the membranes rotate in steady state, friction induces a torque in the rod, and, consequently, a static force is acting on the aluminum block. This force is measured on the balance. (*b*) Inside the test geometry the rod is suspended hanging in two membranes. The membranes rotate with the geometry, and the rod and lever are static.

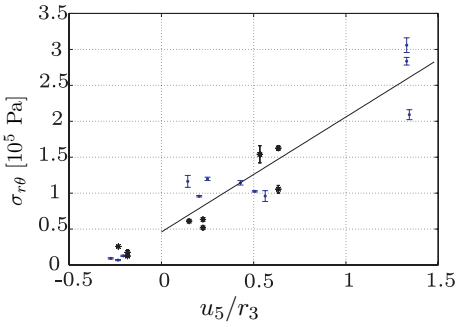

Figure 5. Friction stress in the torque setup for small '•' and large '∗' membrane holes as a function of the displacement u_5/r_3, for different combinations of membrane hole and rod diameter given in table 2. Error bars indicating standard deviations are shown for all data points. The solid line is a linear regression for positive displacements.

torque τ delivered by the friction forces between the rotating silicone membranes and the static rod equals the torque from the reaction force delivered by the aluminum block to the lever. The friction torque τ can thus be calculated as

$$\tau = m_{\text{bal}} g\, L_{\text{lev}} \cos\theta, \tag{4}$$

where L_{lev} is the length of the lever from the rod to the aluminum block, m_{bal} is the mass measured on the balance, θ is the angle between the lever and the surface of the aluminum block and g is the gravitational acceleration. The scaling properties of this type of friction are then analyzed by studying the scaling properties of the friction stress $\sigma_{r\theta}$ given by

$$\sigma_{r\theta} = \frac{\tau}{R_2 A}, \tag{5}$$

where A is the apparent contact area between the steel rod and the silicone membranes.

The geometry of the rotating housing shown in figure 4(*a*) is fabricated in PMMA by drilling and milling processes. The silicone membranes shown in panel (*b*) are 1 mm thick and have an outer diameter of 10 mm. The holes in the membranes are made by a simple punching technique using a steel puncher. Two groups of hole diameters were fabricated, small ones of about 420 μm and large ones of about 740 μm. However, the punching technique does not result in very reproducible holes, which is why the hole diameters had to be measured individually. In table 2, the range of hole diameters as well as the rod diameters is listed.

2.6. Experimental results from the torque setup on scaling of friction

Figure 5 is the main result of the friction studies. It shows the friction stress $\sigma_{r\theta}$ as a function of the relative displacement u_5/r_3, for 25 different combinations of membrane holes and rod diameters listed in table 2. The data points are mean values obtained for one full revolution of the stepper motor. The graph shows that the friction stress depends linearly on the relative displacement u_5/r_3, but does not depend on the apparent contact area. In fact, the area varies by a factor of 4 from 3.1 to 12.4 μm^2 for the 25 measurements. Consequently, the friction force scales linearly with the area. The regression line shown in figure 5 includes only the data points for positive u_5/r_3 values.

Using the slope and intercept of the regression line for $\sigma_{r\theta}$ versus u_5/r_3 together with equations (2) and (3), we obtain the correction factor $k_c = 0.26$ for the torque setup. This is in good agreement with the value $k_c = 0.34$ obtained for the plug setup, see section 2.3. The fact that the measured values of k_c are much smaller than unity can be explained by the difference in geometry and boundary conditions in the actual experiments compared to the simple theoretical model described in section 2.4.

In conclusion, given the linear dependency of the friction stress and relative displacement, and the good agreement in the results for the elastic modulus $k_c k_e$ from the two different test setups, we find it acceptable to proceed using the model summarized in equations (1)–(3) to analyze the turning valve and predict its performance under down-scaling.

3. The turning microvalve

Having obtained a good understanding of the sealing and friction properties of steel rods in silicone microchannels, we now proceed with the design, fabrication and test of the turning microvalve. Based on the analysis in section 2 we employ the following expressions to theoretically predict friction stresses

Table 2. Measured parameters for the torque setup. The thickness of the membrane is $H = 1.0$ mm and the outer membrane diameter is $2r_4 = 1$ cm. Note that a range is given for the diameters of the membrane holes.

Range of the diameter of membrane holes (μm)	Diameter of the rods (μm)			
Small hole: 330–510	250 ± 10	390 ± 10	490 ± 10	740 ± 10
Large hole: 610–870	490 ± 10	740 ± 10	990 ± 10	

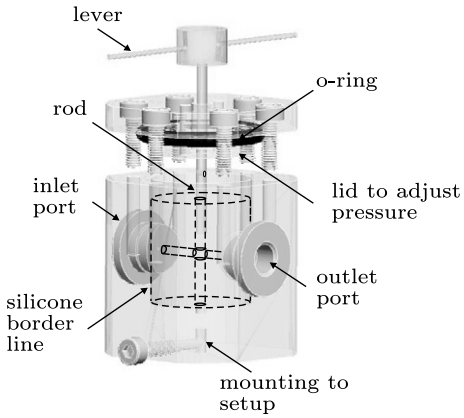

Figure 6. A 3D drawing of the turning valve.

for the turning valve having the elastic modulus k_m:

$$\sigma_{r\theta} = \eta\sigma_{rr}, \tag{6}$$

$$\sigma_{rr} = k_m \frac{u_5}{r_3} + p_0. \tag{7}$$

A lower limit for the threshold pressure p_{th} is given by the plug seal equation

$$p_{\text{th}} = k_m \frac{R_2 - r_3}{r_3} + p_0. \tag{8}$$

Finally, being an important parameter in the design process of portable microsystems, the actuation energy E_{act} of the turning valve, defined for one cycle of opening and closing, is

$$E_{\text{act}} = \tau\pi = \eta\sigma_{rr} A R_2 \, \pi, \tag{9}$$

where τ is the torque and π is the turning angle in radians of two times a quarter turn.

3.1. Design and fabrication of the turning microvalve

To understand the sealing properties of a turning valve we can relate to the experiences made with both the plug setup and the torque setup and adjust those findings according to the boundary conditions imposed by the details of the turning valve design. For example, even though the turning rod displaces the inner channel wall in the same way the plug did in the plug setup, we would predict a higher threshold pressure as compared to a corresponding value of u_1/r_1 in the plug setup. The value will be higher since the outer wall is now supported and hence enhances a self-sealing effect. The analogy to the friction properties of the torque setup is more straightforward, the main difference being that we now have a rod turning in a channel seat instead of a seat of two membrane holes turning around the rod. More subtle differences may arise from the fact that we now have only two edges instead of four.

Figure 6 is a 3D drawing of the turning valve. The valve is constructed using conventional drilling, milling and molding processes. A cavity for the silicone rubber is fabricated in PMMA and is equipped with an adjustable lid. Dashed lines in the figure indicate the border of the silicone part which has been cured around a mold insert in the shape of a cross. The turning rod constitutes one part of the cross, while the other

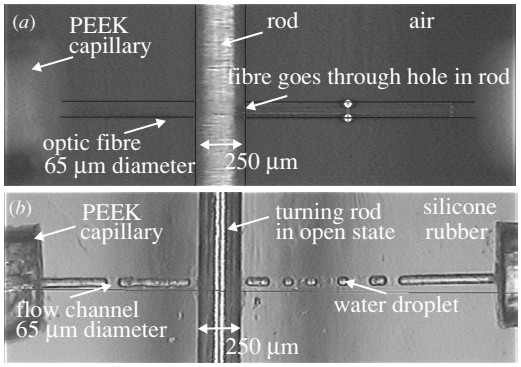

Figure 7. Construction of the channel crossing in a small molded valve. (*a*) Mold insert consisting of a rod, and a transverse fiber going through a hole in the rod and into a receiving PEEK capillary. Air is surrounding the mold insert. The inner diameter of the PEEK capillary is 125 μm. (*b*) Liquid silicone rubber has filled the cavity, and after curing the optical fiber has been pulled out. As a result, a flow channel is created and the rod can freely be turned to open and close for a liquid flow in this channel.

part is created by removing a smaller placeholder rod from the silicone after curing. This smaller rod assures the creation of a fluidic channel and it also keeps the bore in the larger rod free of silicone during the molding and curing process. After removal of the placeholder rod this leaves a channel for liquid flow and a turning valve mechanism to control the flow. When the lid is tightened by means of screws it squeezes the silicone, but due to its incompressible nature the rubber expands into the flow channel and the channel seat containing the turning rod. In that way, the contact force between the rod and the silicone is increased resulting in a larger threshold pressure. In order to control the normal force, the screws in the lid were tightened with a constant-torque Allen wrench.

Two turning valves have been fabricated: a larger one with an outer rod diameter of 1990 μm and a rod channel diameter of 900 μm, and a small one with an outer rod diameter of 250 μm and a rod channel diameter of 65 μm. Figure 7 shows the molding process for the small molded valve. In this case, the mold insert for the flow channel is not a second rod but an optical fiber.

3.2. Experimental results on friction and threshold pressure

The characterization of the turning microvalve was performed using the microfluidic setup and the torque setup as described in sections 2.2 and 2.5, respectively. The valve could be directly incorporated into the flow setup using the inlet and outlet ports for fluidic connection. Also, using a drilled mounting channel shown in figure 6, the valve could be mounted in the torque setup allowing the lever to actuate the balance for torque measurements.

In figure 8, the friction stress $\sigma_{r\theta}$ is plotted versus the relative displacement u_5/r_3. Here we use the same notation as for the torque setup, and as in figure 5 we note that for the geometries of the various turning valves the friction stress does not depend on the contact area but only on the displacement. The friction stress increases linearly until $u_5/r_3 = 0.14$, hereafter it continues to increase linearly albeit at a much slower rate. We shall refer to the conditions $u_5/r_3 \leqslant 0.14$ and

Table 3. Experimental determination of elastic moduli obtained from data fits. The friction coefficient was measured to $\eta = 0.5 \pm 0.1$, and for Poisson's ratio $\sigma = 0.49$ was used.

	k_c	k_e (MPa)	k_m (MPa)	p_0 (MPa)	E (MPa)
Tube	0.34	1.6		0.16	2.4 ± 0.3
Membranes	0.26	2.5		0.092	3.7 ± 0.2
Large valve			0.82	0.023	1.5 ± 0.3
Small valve			0.13	0.12	1.5 ± 0.3

Table 4. Mean values and standard deviation of measured threshold pressure p_{th} for the large and small molded valves, and calculated p_{th} from the simple valve model using equation (8) and using the values of k_m and p_0 from the large turning valve for displacements $u_5/r_3 \leqslant 0.14$. For larger values of the displacement the model valve corresponds to the small valve. It is apparent that for $u_5/r_3 > 0.14$ the model predictions of the threshold pressure are strongly underestimated.

	Displacement u_5/r_3				
	0.13	0.17	0.32	0.41	0.50
p_{th} (MPa), large valve	0	0.18 ± 0.1	0.35 ± 0.2		
p_{th} (MPa), small valve			>0.7	>0.7	>0.7
p_{th} (MPa), model calculation	0.13	0.14	0.16	0.17	0.19

Table 5. Actuation energy E_{act} and other parameters obtained from data fits. The friction coefficient was measured to $\eta = 0.5 \pm 0.1$, and for Poisson's ratio $\sigma = 0.49$ was used. The friction stress is evaluated at $u_5/r_3 = 0.32$.

	Rod diameter (μm)	Contact length (μm)	Nominal area (μm^2)	σ_{r_θ} (MPa)	E_{act} (mJ)
Large valve	1990	23 000	144	0.081	36
Small valve	250	6000	4.76	0.081	0.15
	Stroke volume (μl)	Prestress (10^5 Pa)			E_{act} (mJ)
Check valve	0.160	0.1			1.6×10^{-3}

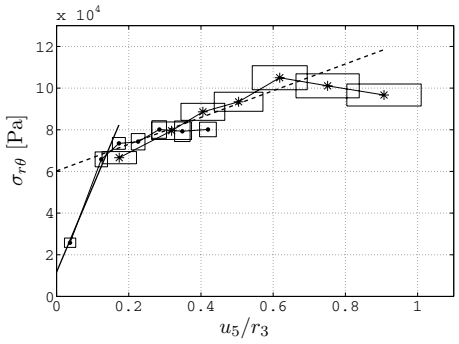

Figure 8. Friction stress for large '•' and small '∗' molded valves as a function of the displacement u_5/r_3. Data points represent mean values of one revolution and boxes indicate uncertainties in both $\sigma_{r\theta}$ and u_5/r_3. For both the large and the small valve, the uncertainties for u_5 and r_3 are 30 and 10 μm, respectively. The solid regression line fits the first three displacements for the large valve, hereafter the torque clings off and reaches a plateau. This plateau is consistent with measurements on the small valve. The dashed line is a fit to the data for the small molded valve. The values of the elastic modulus k_m are listed in table 3 and calculated as the corresponding regression line divided by the friction coefficient η.

$u_5/r_3 > 0.14$ as small and large displacements, respectively. From the linear fits we obtain the elastic modulus for small displacements to $k_m = 0.82$ MPa and the modulus for large displacements to $k_m = 0.13$ MPa, which are used in equation (7).

The results for the various elastic moduli for the plug setup, the torque setup and the turning valve are summarized in table 3. It must be noted that we cannot make a direct comparison of the moduli, as the boundary conditions are different. The silicone rubber in the turning valve is completely confined by a rigid wall and can therefore only expand into the flow channel. For large displacements the friction stress increased more moderately, indicating that we cannot further increase the contact pressure σ_{rr}, even though we increase u_5/r_3. A more thorough finite-element analysis may reveal instabilities due to buckling of the silicone. However, such an analysis is beyond the scope of this work.

From table 4 it is seen that the experimental threshold pressures for the turning valves at $u_5/r_3 > 0.14$ are larger than those obtained by the model calculation based on the plug seal. We can therefore conclude that the turning valves are more efficient than expected. This may be due to the self-sealing effect of the particular geometry. It should also be noted that the small (scaled down) valve is performing better than the large valve.

3.3. Experimental results on the actuation energy

The actuation energy E_{act} is defined by equation (9). If we desire a microvalve with, say, a threshold pressure of at least 0.35 MPa, then according to table 4 a relative displacement of $u_5/r_3 = 0.32$ would be required. Using the results from figure 8 and equation (6) yields a friction stress of $\sigma_{rr} = 0.081$ MPa, and from there via the calculation of the torque we arrive at an actuation energy of $E_{\text{act}} = 36$ mJ. Similarly, for the small turning valve we obtain $E_{\text{act}} = 0.15$ mJ, see also table 5.

In table 5, we also compare the turning valves to a typical check valve in terms of actuation energy. As an

example we have chosen the prestressed inlet check valve from a micropump constructed by Maillefer *et al* [13], and the actuation energy is here calculated as the product of the stroke volume and the opening pressure. Disregarding viscous friction, it is noted that the check valve can be actuated approximately 94 times for the amount of energy required by a turning microvalve. However, the turning valve provides a higher safety level, and it needs only be actuated to change from one state to another. Its energy consumption is thus largely independent of the flow rate and the dosed volumes. Consequently, depending on specific parameters (e.g., stroke volume of the pumps involved) there is a volume threshold above which the turning valve is clearly more economical with regard to energy consumption.

4. Discussion and conclusion

We have studied sealing and friction in elastic silicone-based microchannels and have shown that the friction force scales linearly with the apparent contact area and with the relative displacement of the channel wall. Two turning valves of different sizes constructed from similar materials showed the same linear scaling as well as predictable threshold pressures. It can thus be concluded that it is possible by down-scaling to construct a low-energy valve with a high-pressure seal. Even though the principle of the turning valve is simple and well known, we believe that this is the smallest realization of the valve to date.

The present analysis is based on simple modeling and variations in only a few principal parameters such as size and elastic displacement. Variations in other parameters playing a role for realistic everyday operation conditions, such as temperature and a fast actuation time, have so far been neglected. A more rigorous study on how these parameters influence the performance of the turning valve is desirable and necessary for true robust design.

Acknowledgments

We would like to thank our colleagues at Novo Nordisk Jan Jacobsen, Bjørn G Larsen, Steffen Hansen, Jan Preuthun, Klaus Bendix, Ion M Sivebæk and Gabriel Jørgensen for fruitful discussions on design, fabrication and test.

References

[1] Woias P, Mastrangelo C H and Becker H 2001 *Proc. SPIE* **4560** 39–52
[2] Laser D J and Santiago J G 2004 *J. Micromech. Microeng.* **14** R35–64
[3] Ducrée J and Zengerle R (ed) 2004 *FlowMap Microfluidics Roadmap for the Life Sciences* (Norderstedt, Germany: Books on Demand GmbH)
[4] Taylor W A 1996 *SOCE News, The Society of Concurrent Engineering* (Spring issue) pp 1–6
[5] Quake S A and Scherer A 2000 *Science* **290** 1536–40
[6] Hasselbrink E F, Shepodd T J and Rehm J E 2002 *Anal. Chem.* **74** 4913–8
[7] Kirby B J, Shepodd T J and Hasselbrink E F 2002 *J. Chromatogr.* A **979** 147–54
[8] Frank J A and Pisano A P 2003 *Proc. 12th Int. Conf. on Transducers, Solid-State Sensors, Actuators and Microsystems* vol 1, pp 143–6
[9] Persson B N J, Albohr O, Tartahlino U, Volokitin A I and Tossatti E 2005 *J. Phys.: Condens. Matter* **17** R1–62
[10] Grosch K A 1963 *Proc. R. Soc.* A **274** 21–39
[11] Schallamach A 1952 *Proc. Phys. Soc.* **65** 657–61
[12] Mal A K and Singh S J 1991 *Deformation of Elastic Solids* (Englewood Cliffs, NJ: Prentice-Hall)
[13] Maillefer D, Gamper S, Frehner B, Balmer P, van Lintel H and Renaud P 2001 *Technical Digest: 14th IEEE Int. Conf. on Micro Electro Mechanical Systems (MEMS 2001)* pp 413–17